ACS APPLIED MATERIALS & INTERFACES

Research Article

www.acsami.org

Electronic and Morphological Studies of Conjugated Polymers Incorporating a Disk-Shaped Polycyclic Aromatic Hydrocarbon Unit

Bo He,[†] Benjamin A. Zhang,[†,§] Feng Liu,[‡] Amparo Navarro,[∥] M. Paz Fernández-Liencres,[∥] Ryan Lu,[†] Kelvin Lo,[†,§] Teresa L. Chen,[†] Thomas P. Russell,[‡,⊥] and Yi Liu*[,†]

[†]The Molecular Foundry and [‡]Material Sciences Division, Lawrence Berkeley National Laboratory, One Cyclotron Road, Berkeley, California 94720, United States

[§]Department of Chemistry, University of California, Berkeley, Berkeley, California 94720, United States

[⊥]Department of Polymer Science and Engineering, University of Massachusetts, 120 Governors Drive, Amherst, Massachusetts 01003, United States

[∥]Department of Physical and Analytical Chemistry, Faculty of Experimental Sciences, Universidad de Jaén, Campus Las Lagunillas, E23071 Jaén, Spain

Supporting Information

ABSTRACT: As more research findings have shown the correlation between ordering in organic semiconductor thin films and device performance, it is becoming more essential to exercise control of the ordering through structural tuning. Many recent studies have focused on the influence of side chain engineering on polymer packing orientation in thin films. However, the impact of the size and conformation of aromatic surfaces on thin film ordering has not been investigated in great detail. Here we introduce a disk-shaped polycyclic aromatic hydrocarbon building block with a large π surface, namely, thienoazacoronenes (TACs), as a donor monomer for conjugated polymers. A series of medium bandgap conjugated polymers have been synthesized by copolymerizing TAC with electron donating monomers of varying size. The incorporation of the TAC unit in such semiconducting polymers allows a systematic investigation, both experimentally and theoretically, of the relationships between polymer conformation, electronic structure, thin film morphology, and charge transport properties. Field effect transistors based on these polymers have shown good hole mobilities and photoresponses, proving that TAC is a promising building block for high performance optoelectronic materials.

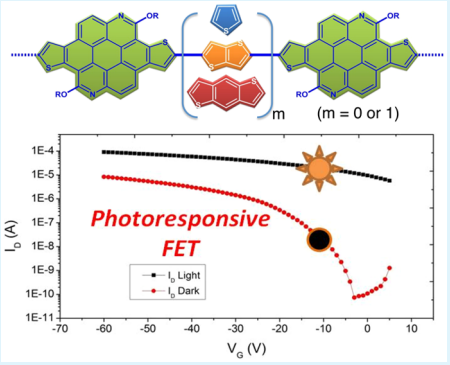

KEYWORDS: *charge transport, morphology, organic semiconductors, polycyclic aromatic hydrocarbon, thienoazacoronene, time-dependent density functional theory*

INTRODUCTION

Organic semiconductors based on conjugated polymers have received increasing attention for their potential application in flexible electronics.[1,2] In the molecular design of high performance conjugated polymers for use in organic field effect transistors (OFETs)[3−10] and organic photovoltaics (OPVs),[11−18] molecular orbital levels alignment, polymer main chain conformation, and side chain engineering are among the most critical considerations.[19−21] Such aspects not only determine the molecular properties of the conjugated polymer but also influence intermolecular interactions that ultimately govern ordering, crystallinity, and crystal orientation in thin films, which have a strong influence on the overall optoelectronic properties and performance in electronic devices.[22] Despite much progress on the synthesis and characterization of conjugated polymers, how to exercise control of ordering and orientation within thin films through structural tuning still remains a challenging task.[23,24] Many recent studies have focused on the influence of side chain engineering on polymer packing in the thin films,[25,26,21] yet the impact of the polymer main chain, consisting of aromatic units with different sizes of π-surfaces, on packing, has not been investigated in great detail. Chen and Frechet and co-workers indicated that more coplanar aromatic surfaces have strong interactions with the underlying substrate due to stronger van der Waals interactions.[27] As a result, the more coplanar polymer chains have a stronger tendency to lie parallel to the substrate and adopt a face-on orientation. The aromatic units that have been employed for comparison in the previous studies, however, have a fairly small size contrast. A more detailed study based on polymers incorporating aromatic units with systematically varied size and larger size differences is desired to gain further insight into the relationship between polymer conformation and packing.

Received: June 4, 2015
Accepted: August 25, 2015
Published: August 25, 2015

DOI: 10.1021/acsami.5b04907
ACS Appl. Mater. Interfaces 2015, 7, 20034−20045

Scheme 1. Synthesis of TAC Polymers

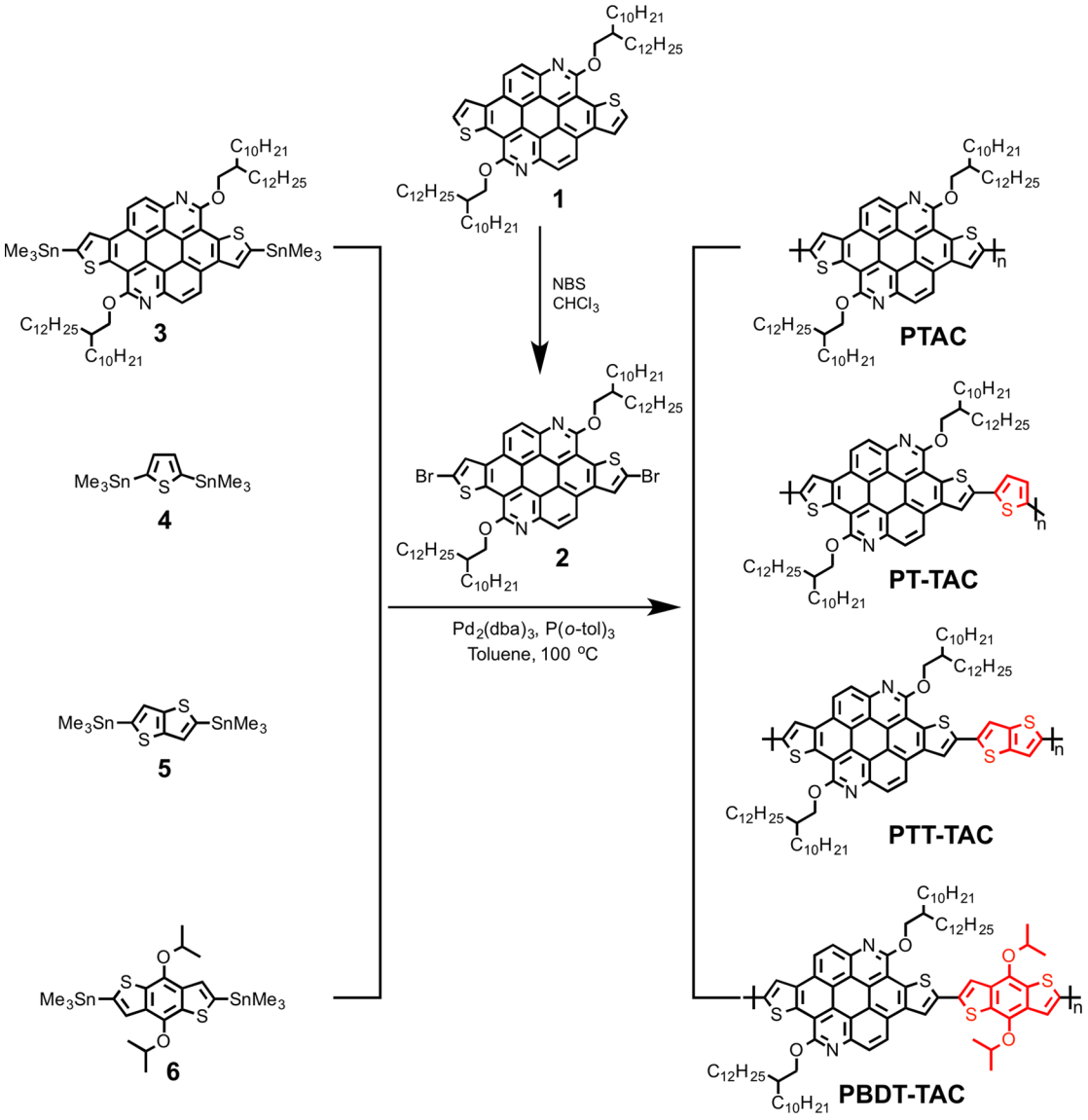

Polycyclic aromatic hydrocarbons (PAHs) are an attractive class of organic semiconductors.[28−30] The large conjugated aromatic surface provides a tunable framework for π electron delocalization, whereas the rigid flat geometry is conducive to influence the tuning of the frontier molecular orbital energies, and the latter is essential for intermolecular charge transport via a hopping mechanism.[31−33] Incorporation of heterocyclic, linear acene-based PAHs into conjugated polymers has been a successful practice to obtain polymers with more rigid conformation and reinforced coplanarity. Acenes ranging from tricyclic to undecyclic ring systems have been incorporated in conjugated polymers.[34] Disk-shaped PAHs based on radially expanded benzenoids are well-known for their excellent self-assembling properties and controllable phase behavior as discotic liquid crystals.[35−37] Their incorporation into the conjugated polymers is expected to impart strong interchain interactions, which will influence solid state packing and optoelectronic properties. Such studies, however, have not been carried out in detail, due to the limited availability of disk-shaped PAH monomers. A few examples of PAH monomers that have been incorporated into conjugated polymers include thiophene fused tetracyclic aromatic units, such as naphthodithiophene and dithienoquinoxaline,[38] and arylene diimides, such as perylene diimide (PDI) and the recent coronene diimide (CDI) units.[39−45]

Thienoazacoroene (TAC) (Scheme 1) is a novel family of disk-shaped heterocyclic PAHs that display well-behaved self-assembly characteristics in the condensed phase.[46] Its structure contains two nitrogen atoms and two regioselectively annulated thiophenes on the coronene core, which is also decorated with two peripheral substituents on the 2,8-position. TAC is particularly suitable for incorporation in conjugated polymers for the following reasons. First, TAC has a relatively low HOMO energy level and electron density, which is mediated by the electron withdrawing nitrogen heteroatoms and the anchoring atoms on the peripheral groups. Second, the trans-annulated thiophenes at the [3,4] and [10,9] positions are free of steric hindrance to the adjacent aromatic units once being incorporated into the polymer backbone, which is important for tuning the polymer bandgap and solid-state packing. Third, the two substitutions on the 2- and 8- positions allow the introduction of solubilizing peripheral groups for good

DOI: 10.1021/acsami.5b04907
ACS Appl. Mater. Interfaces 2015, 7, 20034−20045

solubility and tuning of solid state packing. Finally, TAC can be readily synthesized in large quantity in a few modular and simple steps.

In this paper, TAC was employed as a disk-shaped PAH building block in a series of medium bandgap polymers. Several donor units with varying sizes, including the monothiophene (T), thienothiophene (TT), and benzodithiophene (BDT) moiety were copolymerized with a common TAC moiety. A TAC homopolymer was also prepared for comparison. The optical and electrochemical properties were investigated experimentally and correlated with extensive theoretical modeling results. The charge transporting properties of these polymers were evaluated based on thin film field effect transistor devices. Such polymers show good hole mobilities, suggesting that TAC is a useful building block for high performance organic semiconductor materials. In addition, phototransistors based on one of the polymers exhibit excellent photoresponses. Detailed studies on the thin film morphologies of the TAC polymer series using grazing incidence wide angle scattering (GIWAXS) and atomic force microscopy (AFM) provide insight into the structure−property relationship of molecular structures, morphologies and charge transport properties.

RESULTS AND DISCUSSION

Material Synthesis. TAC monomer was synthesized according to previously reported procedures.[46] The TAC polymers were synthesized by metal-catalyzed polycondensation through Stille coupling reactions. The TAC dibromide **1**[46] was subjected to react with bis-stannyls **2**−**4** to give the TAC homopolymer PTAC, and the alternating donor−donor polymers PT-TAC, PTT-TAC, and PBDT-TAC, respectively. All polymers have good solubility in common organic solvents such as $CHCl_3$ and THF.

Optical and Electrochemical Properties. Optical absorption properties of the TAC polymers were evaluated both in dilute solution and as thin films (Figure 1). The data

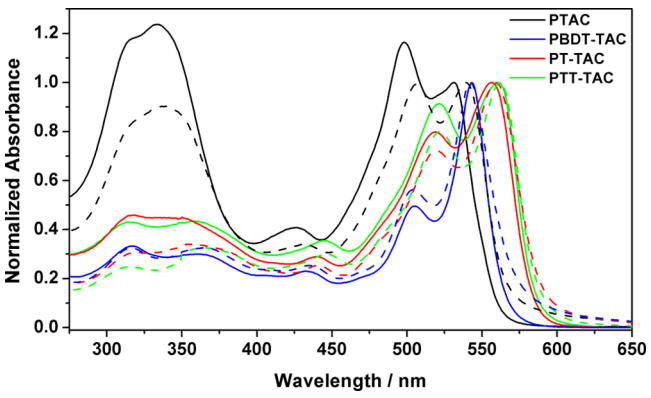

Figure 1. UV−vis absorption spectra of TAC polymers in $CHCl_3$ solution (solid line) and in thin films (dashed line).

are summarized in Table 1. The well-separated vibronic absorption bands of the TAC monomer[46] no longer exist in the polymers. The absorption spectrum of PTAC displays two absorption bands at 480 and 531 nm, which can be assigned to 0−1 and 0−0 transitions, corresponding to a $\pi-\pi^*$ transition and aggregation, respectively. In the spin coated thin film of PTAC, the absorption peaks show bathochromic shifts to 490 and 539 nm, respectively. The bathochromic shift is indicative of more coplanar polymer main chains when moving from solution to the thin film, which is supported by theoretical modeling (see vide infra). The relative peak intensity (I_{0-0}/I_{0-1}) also undergoes notable changes from 0.833 to 1.02, which is an indication of increased aggregation.[47,48] Similar dual-band absorption features were observed for PT-TAC, PTT-TAC, and PBDT-TAC. However, their thin film absorptions displayed negligible shifts when compared to the solution absorption, indicating that there was minimal change of the effective conjugation from solution to thin film. The relative 0−0/0−1 peak intensity increases for thin films of PT-TAC and PTT-TAC, and decreases for PBDT-TAC, suggesting different degrees of aggregation. Although the exact nature remains unclear, we tentatively ascribe the origin of this abnormal trend to the steric hindrance brought about by the isopropoxy substituents on the BDT units. From the absorption edges at the longest wavelength of the thin films, optical bandgaps between 2.09 and 2.16 eV could be estimated for all four polymers (Table 1). The solution photoluminescent spectra of these polymers are plotted in Figure S1 in the Supporting Information.

The electrochemical properties of TAC polymers were investigated in solution (Figure S2 in the Supporting Information) by cyclic voltammetry using the conventional three-electrode setup and ferrocene/ferrocenium (Fc/Fc^+) redox couple as the internal reference. On the basis of the optical and electrochemical data, the energy levels of the HOMOs and LUMOs of all TAC polymers are estimated to be approximately −5.3 and −3.2 eV, respectively (see Table 1).

Theoretical Calculations. Density functional theory (DFT) calculations were performed to predict the optimized geometry of the ground state and the energy associated with the frontier molecular orbitals. Full geometric optimization was carried out on the monomer, dimer, and tetramer of each molecular structure shown in Scheme 1 with n = 1, 2, and 4 to evaluate the impact of different donor units on the molecular structure and electronic properties of TAC polymers. All theoretical calculations were performed using the Gaussian 09 package,[49] version B.01 at the B3LYP/6-31G (d,p)[50,51] level of theory. The excitation energies, oscillator strengths, and configurations involved in the electronic transitions were evaluated using the ground-state optimized geometries and time-dependent density functional theory (TD-DFT). Long alkyl chains were replaced by methyl groups in the calculations to reduce the computational cost.

The energy barrier to rotate about the S−C−C−S torsion angle was calculated for monomers and dimers in order to predict the preferred conformation. As shown in Figures S3 and S4, a near planar trans conformation with the thiophene sulfurs pointing in an opposite direction to the adjacent TAC sulfur atoms was obtained in all cases. The optimized geometries of tetrameric segments of each polymer are given in Figure 2. From these optimized geometries, the torsional angles along the conjugated backbone of the respective oligomers (see Figure 2a for definition) were obtained, listed in Table S1. The torsion angles are found to be in the range of 13° to 17°, except those in the PBDT-TAC polymers, which are typically below 10°, suggesting that there are varying degrees of twisting in these polymers, with PBDT-TAC polymer being the most coplanar.

The frontier molecular orbitals (FMOs) of the tetramers of each polymer are shown in Figure 3 (see Figure S5 for the FMOs of monomers and dimers). HOMO is more delocalized

DOI: 10.1021/acsami.5b04907
ACS Appl. Mater. Interfaces 2015, 7, 20034−20045

Table 1. Summary of Optical and Electrochemical Parameters of TAC Polymers

	UV−vis						cyclic voltammetry[a]		
	solution			film					
compound	λ_{max} (nm)	λ_{max} (nm)	E_g^{opt} (eV)	λ_{max} (nm)	λ_{max} (nm)	E_g^{opt} (eV)	E_{ox}[b] (eV)	HOMO[c] (eV)	LUMO[d] (eV)
PTAC	531	559	2.22	539	565	2.19	0.58	−5.38	−3.16
PT-TAC	556	584	2.12	559	593	2.09	0.46	−5.26	−3.14
PTT-TAC	561	585	2.12	562	592	2.09	0.52	−5.32	−3.20
PBDT-TAC	543	567	2.18	542	575	2.16	0.57	−5.37	−3.19

[a]Measured in solution, using conventional three-electrode setup with a scan rate of 100 mV s^{-1}. [b]The onset of the oxidation potential with respect to the Fc/Fc^+ redox couple. [c]Calculated using $E_{HOMO} = -(4.8 + E_{ox})$ eV. [d]Calculated based on optical bandgap and electrochemical HOMO energy level.

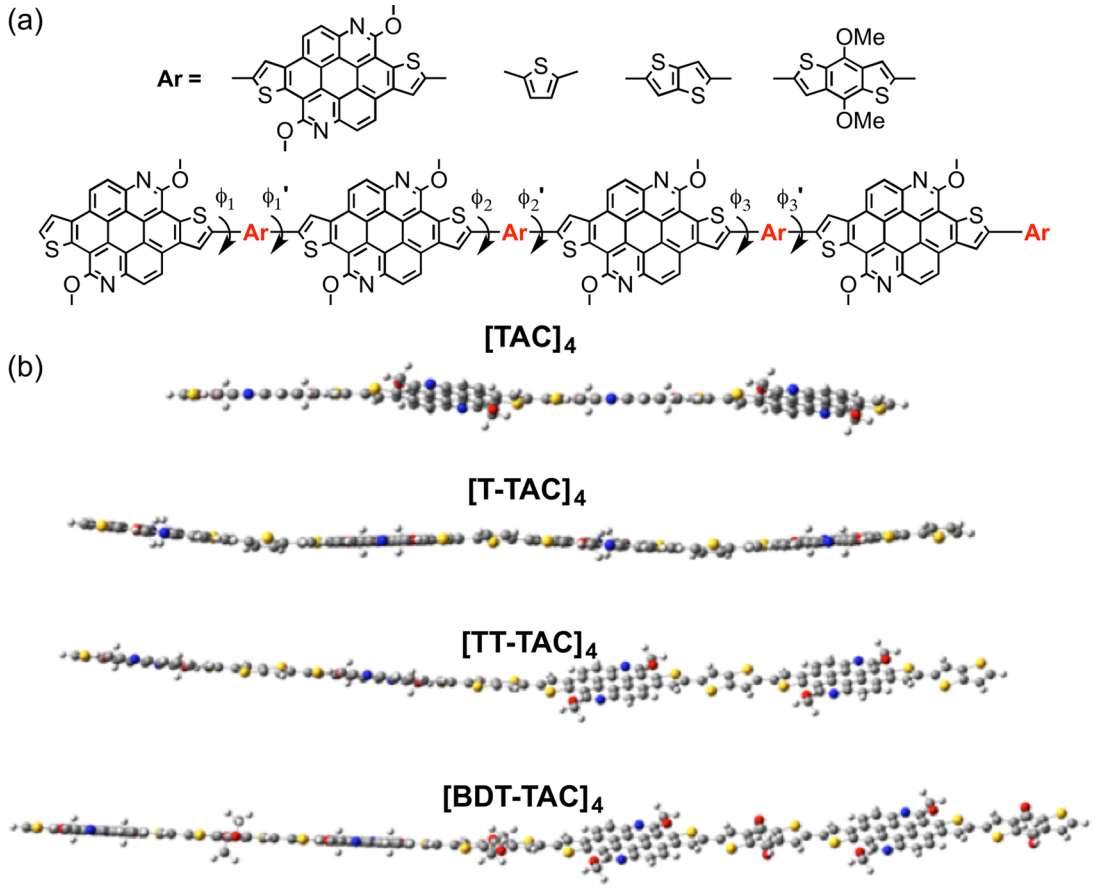

Figure 2. (a) Definition of the torsion angles along the backbone of the oligomers. (b) Molecular representation of the optimized tetramers at the B3LYP/6-31G(d,p) level.

along π-conjugated backbone whereas the LUMO is mainly concentrated on the TAC unit. The HOMO−LUMO energy levels and band gaps for oligomers are shown in Figure 4. The band gaps vary as PTAC > PBDT-TAC > PT-TAC > PTT-TAC, in agreement with experimental data. Not surprisingly, the band gap decreases as the number of repeating units (monomer > dimer > tetramer) increases, due to the extended conjugation, even though the difference between the dimer and tetramer is much smaller than that between the monomer and dimer. In addition, the HOMO level increases and LUMO level decreases from PTAC to the rest of the oligomers. PTT-TAC shows the lowest LUMO and highest HOMO, yielding the narrowest band gap. The respective HOMO and LUMO energy levels for oligomers are given in Table S2.

Table 2 gives the vertical transition energies, oscillator strength, and electronic configuration as determined at the TD-B3LYP/6-31G (d,p) level of theory for the tetramers. The lowest optically allowed electronic transition ($S_0 \rightarrow S_1$) has the largest oscillator strength in all the cases. Also, the $S_0 \rightarrow S_1$ transition can be principally described as the HOMO→LUMO one electron excitation. The results for monomer and dimer are included in Table S3. In general, there is excellent agreement between the experimental data reported in Table 1 and the calculated $S_0 \rightarrow S_1$ vertical transition energies for tetramers, which take values of 2.29, 2.17, 2.14, and 2.20 eV for $[TAC]_4$, $[T\text{-}TAC]_4$, $[TT\text{-}TAC]_4$, and $[BDT\text{-}TAC]_4$, respectively. The oscillator strength is found to increase with the decrease in the torsion angles (coplanarity). Thus, $[BDT\text{-}TAC]_4$ shows the largest value for *f* and $[TAC]_4$ the smallest one.

Additionally, we have explored the impact of the solvent (chloroform) on the computed vertical transition on monomer and dimers by considering the polarizable continuum model

DOI: 10.1021/acsami.5b04907
ACS Appl. Mater. Interfaces 2015, 7, 20034−20045

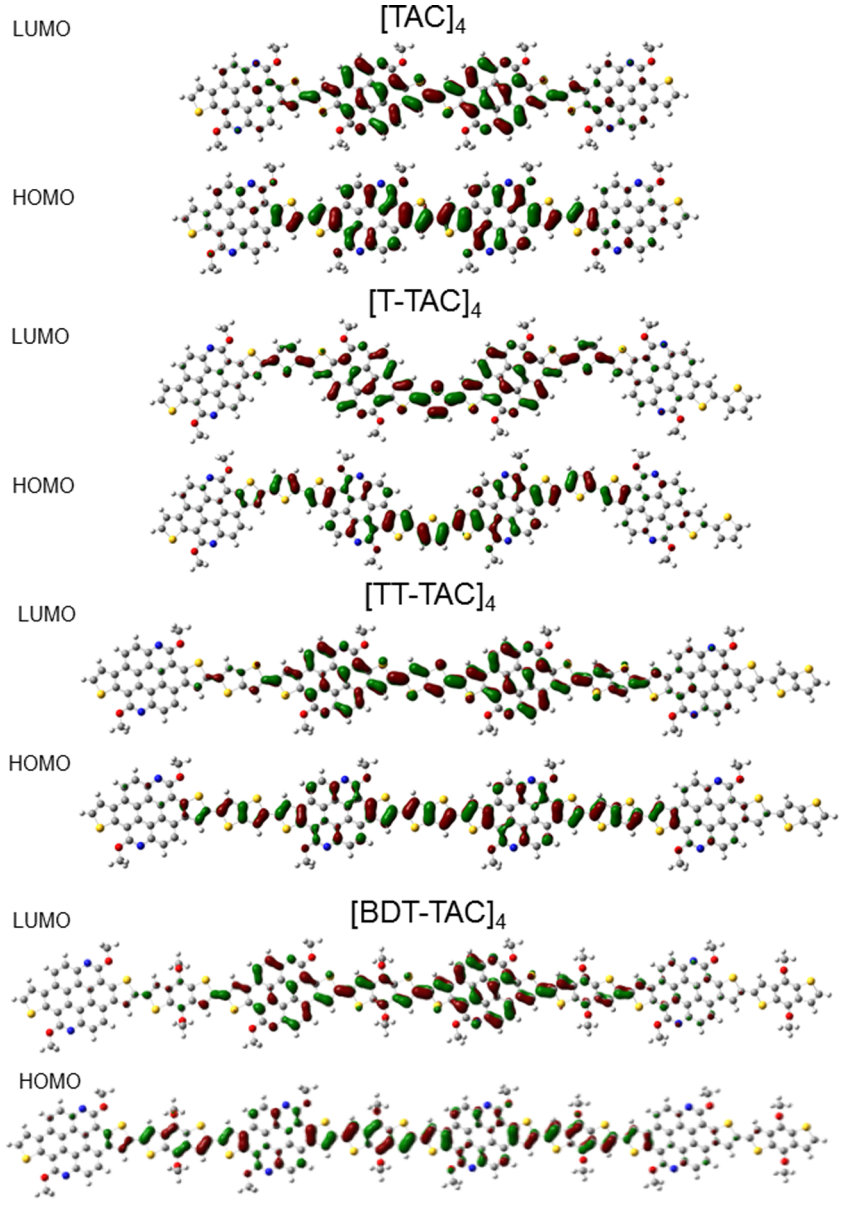

Figure 3. Illustrations of frontier molecular orbitals (isovalue surface 0.02 u.a.) for tetramers of TAC, T-TAC, TT-TAC, and BDT-TAC at the B3LYP/6-31G (d,p) level.

(PCM).[52,53] Geometry optimization and TD-DFT calculations were performed for monomers and dimers at the B3LYP/6-31G (d,p). The torsion angles along the oligomer backbone are collected in Table S4 and HOMO−LUMO energy levels in Table S5. In general, there is a decrease in the torsion angle, that enhances the coplanarity of the backbone. The effect of the solvent in $S_0 \rightarrow S_1$ excitation energy transition is presented in Table S3 (for brevity, only the main contribution is included). As a result, small red shifts ∼0.1 eV were observed for the $S_0 \rightarrow S_1$ transition when the solvent was considered in the calculations.

Furthermore, to verify that the bathochromic shift from solution to film of PTAC is related to higher coplanarity, full optimization of the PTAC tetramer was performed with initial values for the torsion angles $\phi_i, \phi'_i = 0°$. The calculation yields a planar structure for PTAC that is only 0.1 kcal/mol less stable than the twisted structure. The TD-DFT calculation for this planar structure (see data in parentheses in Table 2) yields a small red shift for $S_0 \rightarrow S_1$ transition from 541 to 548 nm (∼7 nm), in agreement with the experimental data. The HOMO and LUMO molecular orbitals shown in Figure S6 are very similar to those for the twisted structure. Therefore, according to our calculations, PTAC could adopt a more planar conformation when the polymer chain goes from solution to solid state, which could provide the origin of the red shift observed in PTAC.

Morphological Studies. Grazing incident wide-angle X-ray scattering (GIWAXS) measurements were conducted to probe the molecular packing within the spin coated films of TAC polymers. Distinctively different GIWAXS patterns were observed for these polymers (Figure 5a). Out-of-plane and in-plane line-cut profiles are summarized in Figure 5b,c for the annealed samples. The as-spun thin film of PTAC showed a diffuse reflection characteristics of the $\pi-\pi$ stacking and out-of-plane (h00) (h up to 3) reflections, in keeping with an edge-on lamellar packing. Upon annealing at 175 °C for 10 min and

DOI: 10.1021/acsami.5b04907
ACS Appl. Mater. Interfaces 2015, 7, 20034−20045

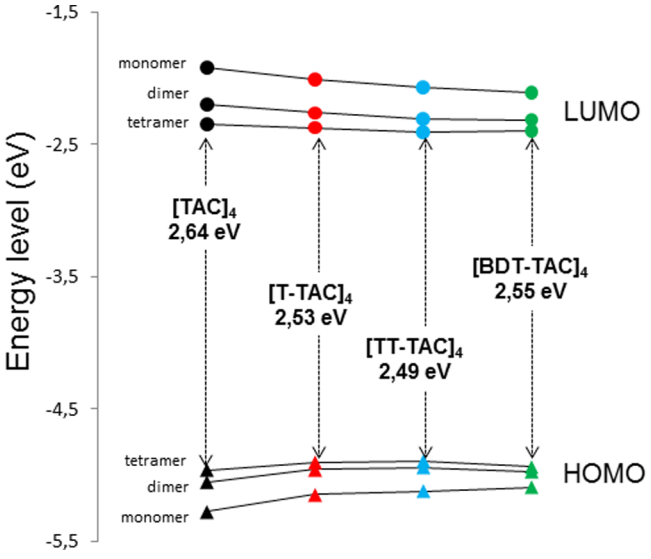

Figure 4. Energies of HOMO (triangles) and LUMO (circles) calculated at the B3LYP/6-31G (d,p) level (black, TAC; red, T-TAC; blue, TT-TAC; green, BDT-TAC).

cooling to room temperature, the structural order of the film was greatly improved. Higher order (h00) (h up to 4) reflections became more pronounced, indicating enhanced crystallinity of the film. The angular distribution of the (010) reflection, characteristic of the $\pi-\pi$ stacking (3.55 Å), became much narrower and clearly evident in the plane of the film, indicating that a better edge-on orientation was achieved. PT-TAC showed a similar signature of GIWAXS pattern for the as-spun thin film. Thermal annealing led to enhanced structural order and crystal orientation. However, in this case, the enhanced $\pi-\pi$ stacking peaks became narrower and centered in both in-plane and out-of-plane direction (3.46 Å), corresponding to PT-TAC chains forming edge-on and face-on crystalline lamellae. It should be noted that the (100) peak for PTAC and PT-TAC is not a single Gaussian but rather two peaks merging in close spacing, suggesting that the polymers are polymorphic. PTT-TAC showed quite broad (100) and (010) peaks in as-spun film. The azimuthal distribution of the in-plane $\pi-\pi$ stacking peak (3.50 Å) became narrower upon annealing, together with more pronounced out-of-plane reflections due to enhanced crystallinity. In contrast to PTAC and PTT-TAC polymers, GIWAXS pattern of the pristine thin film of PBDT-TAC displayed a very strong out-of-plane $\pi-\pi$ stacking peak (3.58 Å), suggesting that the polymer lamellae have a dominantly face-on orientation. These peaks became more pronounced upon annealing. Noticeably, the weak in-plane π-stacking peaks started to intensify upon thermal annealing. A comparison of the $\pi-\pi$ stacking distances and crystal size, as determined from a Scherrer analysis, for these annealed samples was also carried out. PT-TAC polymer showed the smallest $\pi-\pi$ distance of 3.46 Å and a crystal size of 4.69 nm. PTT-TAC showed a $\pi-\pi$ stacking distance of 3.50 Å and a crystal size of 5.21 nm. The homopolymer PTAC showed a $\pi-\pi$ stacking distance of 3.55 Å and a crystal size of 3.81 nm. It appears that adjusting the separation between intrachain TAC monomers could lead to a stronger intermolecular packing, which will subsequently impact charge transport within the thin films. PBDT-TAC polymer showed a $\pi-\pi$ stacking distance of 3.58 Å with a crystal size of 2.88 nm. The branched isopropoxy substitution on BDT unit presumably weakens the interaction between polymer chains, leading to very different microstructures within the thin film.

The origin of the different orientations of lamellae is an active subject of study. Side chain/substrate interactions have been indicated as an important factor in determining the orientation of the π-stacks.[47] For the TAC-based polymer series, only PBDT-TAC carries two types of side chains whereas PTAC, PT-TAC, and PTT-TAC share the same ODT side chains. However, because the isopropoxy side chain on the BDT unit is much shorter than the ODT side chain, the isopropoxy groups can be considered as spatially isolated from

Table 2. Vertical Transition Energy, Wavelength, Oscillator Strength and Electronic Configuration Determined with TD-B3LYP/6-31G(d,p) for Tetramer[a]

tetramer	transition	energy (eV)	absorption (nm)	f	contribution (%)
$[TAC]_4$	$S_0 \rightarrow S_1$	2.29 (2.26)[b]	541 (548)[b]	3.80 (3.85)[b]	H→L (88)
	$S_0 \rightarrow S_4$	2.68 (2.66)[b]	463 (466)[b]	0.59 (0.64)[b]	H−1→L+1 (63, 65[b])
$[T\text{-}TAC]_4$	$S_0 \rightarrow S_1$	2.17	570	5.09	H→L (81)
					H−1→L+1 (12)
	$S_0 \rightarrow S_4$	2.51	494	0.72	H−1→L+1 (55)
					H→L+2 (21)
$[TT\text{-}TAC]_4$	$S_0 \rightarrow S_1$	2.14	581	6.57	H→L (78)
					H−1→L+1 (14)
	$S_0 \rightarrow S_2$	2.29	541	0.01	H−1→L (45)
					H→L+1 (46)
	$S_0 \rightarrow S_4$	2.45	506	0.84	H−1→L+1 (50)
					H→L+2 (21)
$[BDT\text{-}TAC]_4$	$S_0 \rightarrow S_1$	2.20	563	7.22	H→L (72)
					H−1→L+1 (17)
	$S_0 \rightarrow S_2$	2.32	535	0.01	H−1→L (44)
					H→L+1 (72)
	$S_0 \rightarrow S_3$	2.45	506	0.62	H−2→L (38)
					H−1→L+1 (14)
					H→L+2 (22)

[a]Transition with $f \geq 0.01$. [b]Data in parentheses corresponds to planar structure.

DOI: 10.1021/acsami.5b04907
ACS Appl. Mater. Interfaces 2015, 7, 20034−20045

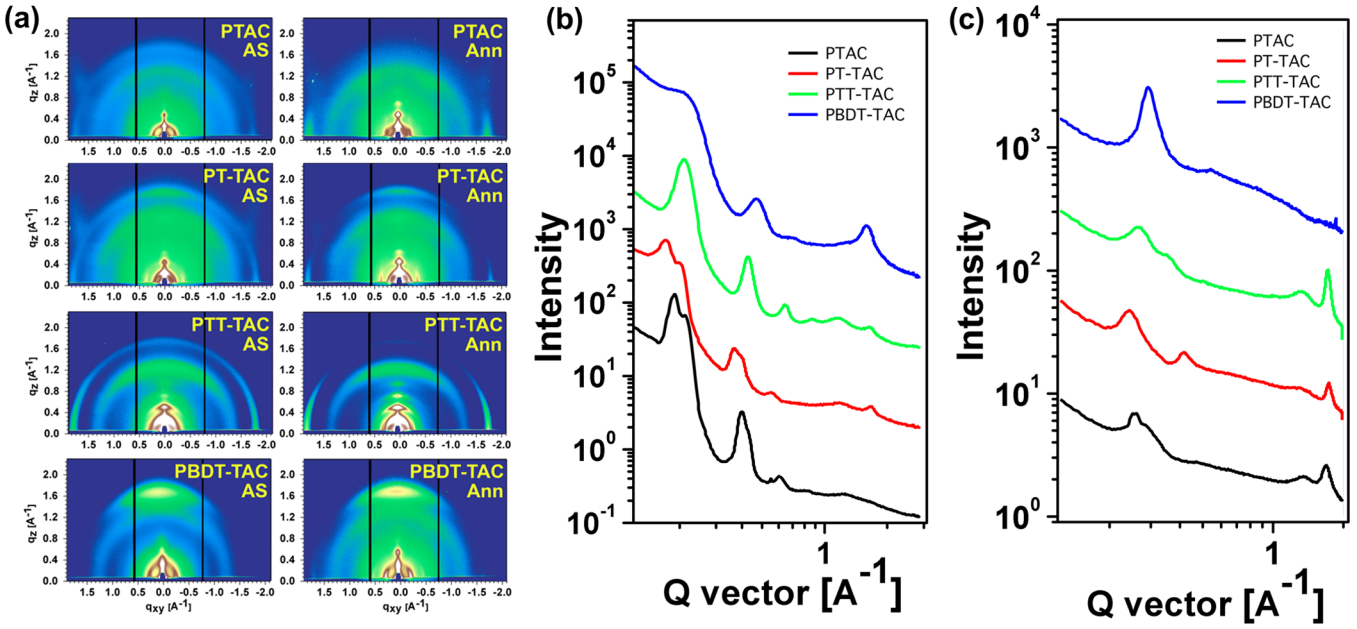

Figure 5. (a) GIWAXS patterns of thin films of the polymers before (left) or after annealing (right). (b) Out-of-plane and (c) in-plane line-cut profiles.

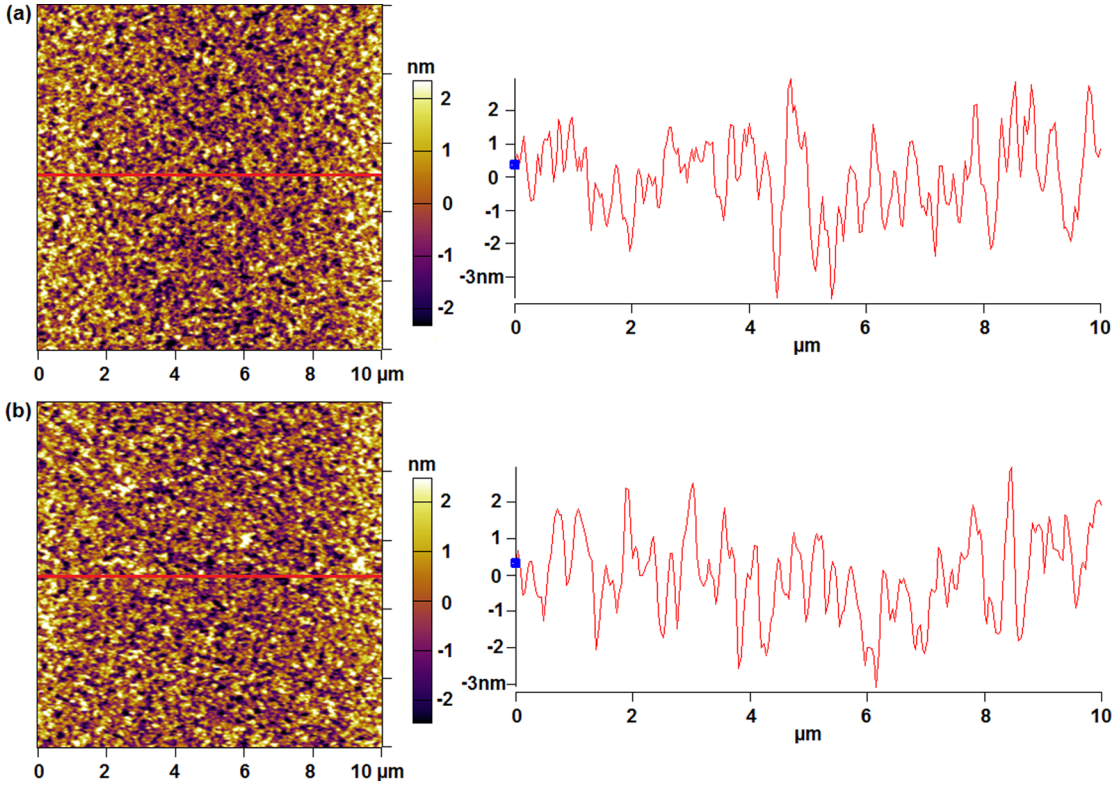

Figure 6. AFM images and line profiles of spuncast PT-TAC thin films (a) before annealing and (b) after annealing. Annealing temperature was 175 °C.

any underlining substrate due to the size mismatch. Thus, the side chain/substrate interfaces are similar for the four TAC polymers, which cannot account for the different orientations of the polymer microcrystalline domains. Another consideration is the influence of attached side chain density. According to DeLongchamp and co-workers,[54] different side chain densities on the polymer conjugated backbone is responsible for the preferred orientation, with the higher side chain density yielding the face-on conformation and the lower side chain density more prone to giving rise to an edge-on orientation. This trend is, however, not observed in current polymer series. On the basis of the relative length of the aromatic units, PTAC has the highest side chain density, followed by PT-TAC and PTT-TAC. PBDT-TAC has the lowest density, not taking the isopropoxy group into consideration. In contrast to the previously suggested trend, PTAC with the highest side-chain

DOI: 10.1021/acsami.5b04907
ACS Appl. Mater. Interfaces 2015, 7, 20034−20045

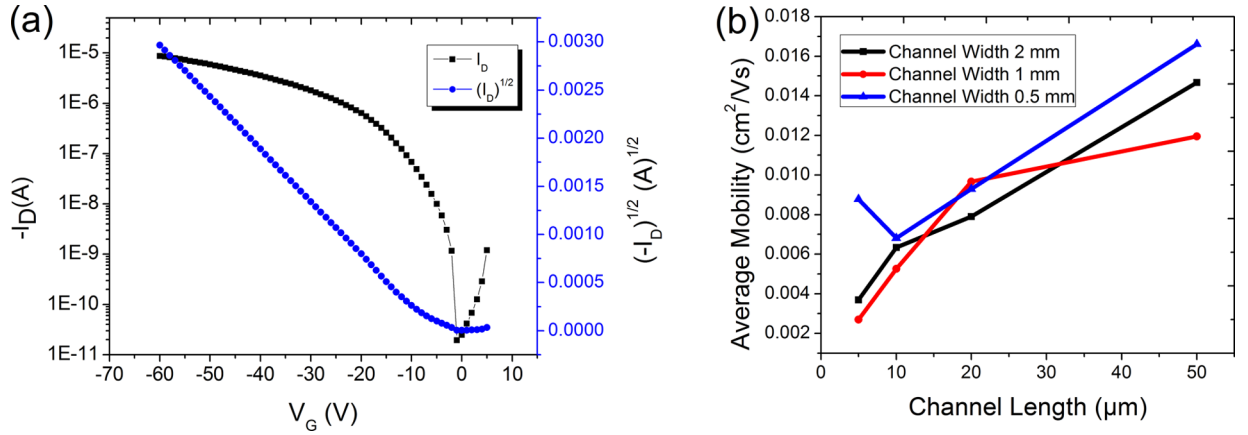

Figure 7. (a) Representative transfer curve of PT-TAC FET devices (BGTC). (b) Average mobilities of PT-TAC polymers measured in BGBC devices with different channel lengths and widths.

Table 3. OFET and SCLC Device Characteristics of TAC Polymers

	pristine (cm^2 V^{-1} s^{-1})			annealed (cm^2 V^{-1} s^{-1})				
compound	$\mu_h^{max,a}$	$\mu_h^{ave,b}$	$\mu_{sclc}^{ave,c}$	$\mu_h^{max,a}$	$\mu_h^{ave,b}$	$\mu_{sclc}^{ave,c}$	V_{th}[e]	I_{On}/I_{Off}[e]
PTAC	–[d]	–[d]	9.7×10^{-6}	1.4×10^{-3}	1.3×10^{-3}	2.9×10^{-5}	−15	10^3
PT-TAC	8.9×10^{-3}	8.8×10^{-3}	3.6×10^{-4}	4.3×10^{-2}	3.4×10^{-2}	2.3×10^{-4}	−11	10^5
PTT-TAC	3.9×10^{-4}	2.4×10^{-4}	1.9×10^{-5}	2.0×10^{-3}	1.3×10^{-3}	3.5×10^{-6}	−14	10^3
PBDT-TAC	1.1×10^{-4}	1.1×10^{-4}	1.9×10^{-5}	3.1×10^{-4}	2.6×10^{-4}	3.3×10^{-5}	−4.1	10^3

[a]Maximum OFET hole mobility. [b]Average OFET hole mobility. The average mobility was obtained from a minimum of 3–9 pixels from 1 to 3 different chips. [c]Average SCLC mobility from 8 devices. [d]No working devices could be obtained. [e]Characteristics of OFET devices.

density adopts a preferred edge-on orientation, whereas PBDT-TAC with the lowest side-chain density has a preferred face-on orientation. In addition, PT-TAC shows a higher tendency of forming face-on π-stacks than PTT-TAC, further suggesting no correlation between the side chain density and the π-stacking orientation preference. It can be thus inferred that the side-chain/substrate interaction is not the sole interaction in governing the orientation preference. Instead, the polymer main chain/substrate interaction is likely to play a significant role. Size and coplanarity of the π-backbone are two major factors to consider. It is clear that larger π-surfaces alone do not mandate a strong face-on polymer orientation on the substrate, judging from the edge-on orientation observed in PTAC film. On the other hand, the most coplanar PBDT-TAC preferentially adopts a face-on orientation, which is consistent with Chen and Frechet and co-workers' observations[27] that the more coplanar π-surface favors a face-on orientation. These suggest that it is the coplanarity rather than the size of the aromatic backbone dictates the face-on polymer orientation. The data also indicates that a face-on conformation is a metastable state that transforms to the thermodynamically more stable edge-on conformation upon annealing.[54]

Atomic force microscopy (AFM) images of the pristine, and annealed films show the formation of fiber-like intercalating networks (Figure 6 and Figure S7). Consistent with thermally induced molecular reorganization and changes of molecular packing within the films, the roughness increased slightly after annealing in each case. The film roughnesses are between 0.832 and 1.67 nm, increasing in roughness as PTT-TAC < PBDT-TAC < PT-TAC < PTAC.

OFET and SCLC Mobilities Measurement. All four TAC-polymers behave as *p*-type semiconductors in thin film OFET devices. The devices were fabricated using either a bottom-gate, top-contact electrode (BGTC) or bottom-gate, bottom-contact (BGBC) geometry. The polymer thin films were prepared by spin coating and either used as is or annealed at 175 °C for 30 min unless noted otherwise. In general, the annealed devices display higher performances than the pristine ones. A temperature-dependent study of PT-TAC indicated that these films annealed at 175 °C exhibit the highest mobility (Table S6 in the Supporting Information). Among all the BGTC devices annealed under the same conditions, PT-TAC exhibits the highest hole mobility with an average value of 0.034 cm^2 V^{-1} s^{-1}. Both the PTAC and the PTT-TAC polymers have an intermediate average mobility of 1.3×10^{-3} cm^2 V^{-1} s^{-1} and PBDT-TAC polymer has the lowest average mobility of 2.6×10^{-4} cm^2 V^{-1} s^{-1}. The transfer and output curves are shown in Figure 7 and Figure S8, and full device characteristics are listed in Table 3. On the other hand, the vertical charge transport mobilities were measured by space charge limited current (SCLC) methods (Table 3). For the as-cast films, PTAC, PTT-TAC, and PBDT-TAC have similar SCLC mobilities around 1 to 2×10^{-5}. PT-TAC has a mobility 1 order of magnitude higher at 3.6×10^{-4}. Their SCLC mobilities are relatively insensitive to thermal treatment except for PTT-TAC, which decreases almost 5 times after annealing.

PT-TAC was also used as the active material for the fabrication of BGBC devices. Different electrode geometries were used to investigate the influence of channel length and width on charge transport properties. As shown in Figure 7b, the plots indicated the correlation between channel length and hole mobility at various channel widths, showing nearly a monotonic increase of mobility with increasing channel length. It has been reported previously that larger contact resistance at smaller channel lengths[55] or small areas of disordered film localized near the bottom contacts leads to decreased mobilities.[56] The observed nearly monotonic increase in mobility indicates that the devices are not limited by crystalline

DOI: 10.1021/acsami.5b04907
ACS Appl. Mater. Interfaces 2015, 7, 20034–20045

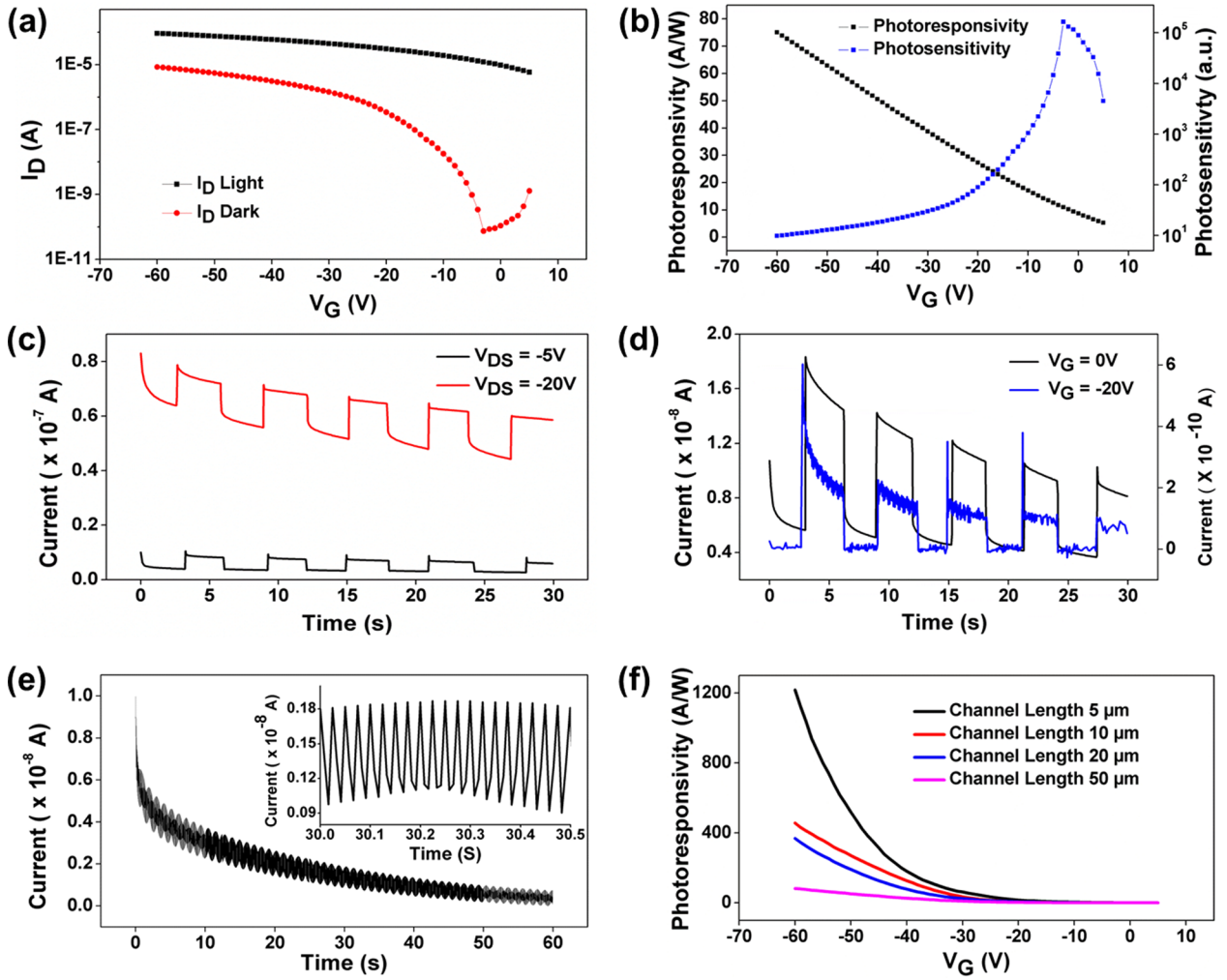

Figure 8. (a) Transfer characteristics of PT-TAC under illumination at 370 μW/cm^2. (b) Photosensitivity (P) and photoresponsivity (R) of PT-TAC measured in the BGTC geometry. (c) Photoswitching behavior at a gate bias of −20 V and source−drain biases of −5 and −20 V. (d) Photoswitching at a source drain bias of −20 V and gate bias of 0 and −20 V. (e) Extended on−off switching of device with 5 ms light pulse intervals. (f) Photoresponsivity of PT-TAC-based OFETs (BGBC) at various channel lengths.

defects and grain boundaries within the crystalline film in the channel.[57]

The transport properties of these polymers qualitatively correlate with the different packing and orientations of the polymer chains shown by GIWAXS. The PBDT-TAC polymer has the lowest OFET mobility, owing to the dominant face-on orientation of the polymer lamellae that is less favorable for lateral charge transport in FETs. PTAC, PT-TAC, and PTT-TAC that have edge-on lamellar morphologies exhibit higher OFET mobilities. Interestingly, PT-TAC with a bimodal orientation distribution has a higher mobility than PTAC and PTT-TAC that possess a more dominant edge-on phase. This is consistent with DeLongchamp and co-workers' observations,[54] which suggests that there are more effective intercalated charge conduction pathways in crystalline domains with bimodal orientation distributions. Such bimodal distribution in PT-TAC also explains its higher SCLC mobility than PBDT-TAC, despite that the latter has a more pronounced face-on orientation preference. On the other hand, PTT-TAC has the lowest SCLC mobility, consistent with its lack of face-on chain packing in the annealed thin film.

Phototransistors of PT-TAC. We also investigated the phototransistor behavior of the PT-TAC polymer. The difference in transfer characteristics of PT-TAC between dark and irradiated BGTC devices is shown in Figure 8a. Under irradiation, PT-TAC displays a large increase in current due to photogeneration of excitons that dissociate under the applied electric potential.[58] This leads to an enhanced hole mobility of 0.11 cm^2 V^{-1} s^{-1}. The device exhibits a high off current under extended irradiation, resulting in a decrease in on/off ratio to 1.8 × 10^3 and in V_t to −5.7 V. Photosensitivity (P) and photoresponsivity (R) of the transistor were calculated using the following equations:

$$P = \frac{I_{\text{Light}} - I_{\text{Dark}}}{I_{\text{Dark}}} \quad (1)$$

$$R = \frac{I_{\text{Light}} - I_{\text{Dark}}}{E_{\text{Light}} * A} \quad (2)$$

where I_{Light} is the current under irradiation, I_{Dark} is the dark current, E_{Light} is the irradiance of the light source (μW/cm^2), and A is the channel area.[59] The large difference in dark and light current yields an appreciable photosensitivity and photoresponsivity, with a maximum of 1.8 × 10^5 and 75 A/W, respectively (Figure 8b).

DOI: 10.1021/acsami.5b04907
ACS Appl. Mater. Interfaces 2015, 7, 20034−20045

Pulsing light in intervals of 3 s under constant gate bias yields an increased overall current density at different drain-source biases. Figure 8c shows the current plots at a constant gate bias of −20 V and source-drain biases of −5 and −20 V, respectively. The ratio between light and dark current is in the range of 10^1−10^2. At a lower gate voltage of 0 V, similar light pulse leads to a lower current but an increased light-to-dark current ratio (~10^3) in accordance with high photosensitivity at low gate voltages (Figure 8d). Furthermore, the phototransistor devices display rapid response to light, as shown by the reversible photoswitching behavior when irradiated with light pulsed at 5 ms intervals (Figure 8e). Finally, the channel length dependence of the photoresponse was also investigated for the BGBC devices. The photoresponsivity increases significantly from 80 to 1200 A/W as the channel length decreases from 50 to 5 μM (Figure 8f). This is consistent with previous reports.[58] Overall, PT-TAC has demonstrated well-behaved phototransistor properties, such as high photoresponsivity and good photosensitivity, which are comparable to the highest values reported for polymer thin film transistors[60−62] and can be further tuned by changing the device geometry and the applied gate biases.

CONCLUSIONS

Thienoazacoronene derivatives, disk-shaped PAH donor units that possess a large aromatic surface, have been utilized for the construction of semiconducting conjugated polymers. The copolymerization with a series of aromatic units readily gives rise to a series of structured medium-gap polymers. In-depth analysis of their thin film morphologies and charge transport properties, together with TD-DFT calculations, have validated several structure−property relationship hypotheses. As evidenced by GIWAXS, these polymers showed a well-behaved yet distinctive self-assembly behavior in thin films arising from the TAC unit. Lamellar structures with edge-on, face-on, or mixed phases were obtained with thermal processed films, which allowed a detailed analysis of the influence of side chain and polymer main chain on orientation preferences of π-stacks. Our findings have indicated that side chain−substrate interactions are not the dominating factor for the observed orientation preference. On the other hand, coplanarity rather than the size of the aromatic surfaces of the polymer backbone is more favorable in guiding a face-on orientation. The polymers display good *p*-type carrier transport mobility in spuncast thin film FET devices. In addition, phototransistors fabricated from PT-TAC show great responsiveness and sensitivity to light, suggesting that light irradiation can be used as another effective means to control the on and off states of the transistor.

ASSOCIATED CONTENT

Supporting Information

The Supporting Information is available free of charge on the ACS Publications website at DOI: 10.1021/acsami.5b04907.

Synthesis and characterization of the precursors and polymers. Cyclic voltammetry. OFET transfer and output curves. Molecular modeling of the oligomers (PDF).

AUTHOR INFORMATION

Corresponding Author

*Y. Liu. E-mail: yliu@lbl.gov.

Author Contributions

The paper was written through contributions of all authors. All authors have given approval to the final version of the paper.

Funding

Department of Energy, Office of Basic Energy Sciences

Notes

The authors declare no competing financial interest.

ACKNOWLEDGMENTS

This work was performed at the Molecular Foundry, partly supported by Self-Assembly of Organic/Inorganic Nanocomposite Materials program (B.H. and Y.L.), with the X-ray experiment conducted at the Advanced Light Source (ALS), Lawrence Berkeley National Laboratory, all supported by the Office of Science, Office of Basic Energy Sciences, of the U.S. Department of Energy under Contract No. DE-AC02-05CH11231. F.L. and T.P.R. were supported by Polymer-Based Materials for Harvesting Solar Energy (PHaSE), an Energy Frontier Research Center funded by the U.S. Department of Energy, Office of Basic Energy Sciences under award number DE-SC0001087. We thank David Hanifi at Stanford for providing the substrates for BGBC devices. Financial support from Junta de Andalucía (FQM337) and Computational resources supplied by the Centro de Servicios de Informática y Redes de Comunicaciones (CSIRC-Universidad de Granada, Spain) are acknowledged.

REFERENCES

(1) Kelley, T. W.; Baude, P. F.; Gerlach, C.; Ender, D. E.; Muyres, D.; Haase, M. A.; Vogel, D. E.; Theiss, S. D. Recent Progress in Organic Electronics: Materials, Devices, and Processes. *Chem. Mater.* **2004**, *16*, 4413−4422.

(2) Facchetti, A. Organic Semiconductors: Made to Order. *Nat. Mater.* **2013**, *12*, 598−600.

(3) Wang, C.; Dong, H.; Hu, W.; Liu, Y.; Zhu, D. Semiconducting Π-Conjugated Systems in Field-Effect Transistors: A Material Odyssey of Organic Electronics. *Chem. Rev.* **2012**, *112*, 2208−2267.

(4) Takeda, Y.; Andrew, T. L.; Lobez, J. M.; Mork, A. J.; Swager, T. M. An Air-Stable Low-Bandgap N-Type Organic Polymer Semiconductor Exhibiting Selective Solubility in Perfluorinated Solvents. *Angew. Chem., Int. Ed.* **2012**, *51*, 9042−9046.

(5) Dong, H.; Fu, X.; Liu, J.; Wang, Z.; Hu, W. 25th Anniversary Article: Key Points for High-Mobility Organic Field-Effect Transistors. *Adv. Mater.* **2013**, *25*, 6158−6183.

(6) Li, H.; Kim, F. S.; Ren, G.; Jenekhe, S. A. High-Mobility N-Type Conjugated Polymers Based on Electron-Deficient Tetraazabenzodifluoranthene Diimide for Organic Electronics. *J. Am. Chem. Soc.* **2013**, *135*, 14920−14923.

(7) Mei, J.; Diao, Y.; Appleton, A. L.; Fang, L.; Bao, Z. Integrated Materials Design of Organic Semiconductors for Field-Effect Transistors. *J. Am. Chem. Soc.* **2013**, *135*, 6724−6746.

(8) Zhao, Y.; Guo, Y.; Liu, Y. 25th Anniversary Article: Recent Advances in N-Type and Ambipolar Organic Field-Effect Transistors. *Adv. Mater.* **2013**, *25*, 5372−5391.

(9) Cai, Z.; Luo, H.; Qi, P.; Wang, J.; Zhang, G.; Liu, Z.; Zhang, D. Alternating Conjugated Electron Donor−Acceptor Polymers Entailing Pechmann Dye Framework as the Electron Acceptor Moieties for High Performance Organic Semiconductors with Tunable Characteristics. *Macromolecules* **2014**, *47*, 2899−2906.

(10) Lei, T.; Xia, X.; Wang, J.-Y.; Liu, C.-J.; Pei, J. Conformation Locked" Strong Electron-Deficient Poly(P-Phenylene Vinylene) Derivatives for Ambient-Stable N-Type Field-Effect Transistors: Synthesis, Properties, and Effects of Fluorine Substitution Position. *J. Am. Chem. Soc.* **2014**, *136*, 2135−2141.

(11) Thompson, B. C.; Frechet, J. M. J. Polymer-Fullerene Composite Solar Cells. *Angew. Chem., Int. Ed.* **2008**, *47*, 58−77.

(12) Brédas, J.-L.; Norton, J. E.; Cornil, J.; Coropceanu, V. Molecular Understanding of Organic Solar Cells: The Challenges. *Acc. Chem. Res.* **2009**, *42*, 1691−1699.
(13) Cheng, Y.-J.; Yang, S.-H.; Hsu, C.-S. Synthesis of Conjugated Polymers for Organic Solar Cell Applications. *Chem. Rev.* **2009**, *109*, 5868−5923.
(14) Cabanetos, C.; El Labban, A.; Bartelt, J. A.; Douglas, J. D.; Mateker, W. R.; Fréchet, J. M. J.; McGehee, M. D.; Beaujuge, P. M. Linear Side Chains in Benzo[1,2-B:4,5-B′]Dithiophene−Thieno[3,4-C]Pyrrole-4,6-Dione Polymers Direct Self-Assembly and Solar Cell Performance. *J. Am. Chem. Soc.* **2013**, *135*, 4656−4659.
(15) Kularatne, R. S.; Magurudeniya, H. D.; Sista, P.; Biewer, M. C.; Stefan, M. C. Donor−Acceptor Semiconducting Polymers for Organic Solar Cells. *J. Polym. Sci., Part A: Polym. Chem.* **2013**, *51*, 743−768.
(16) Huang, Y.; Kramer, E. J.; Heeger, A. J.; Bazan, G. C. Bulk Heterojunction Solar Cells: Morphology and Performance Relationships. *Chem. Rev.* **2014**, *114*, 7006−7043.
(17) Li, Y.; Yao, K.; Yip, H.-L.; Ding, F.-Z.; Xu, Y.-X.; Li, X.; Chen, Y.; Jen, A. K. Y. Eleven-Membered Fused-Ring Low Band-Gap Polymer with Enhanced Charge Carrier Mobility and Photovoltaic Performance. *Adv. Funct. Mater.* **2014**, *24*, 3631−3638.
(18) Warnan, J.; Cabanetos, C.; Bude, R.; El Labban, A.; Li, L.; Beaujuge, P. M. Electron-Deficient N-Alkyloyl Derivatives of Thieno-[3,4-C]Pyrrole-4,6-Dione Yield Efficient Polymer Solar Cells with Open-Circuit Voltages > 1 V. *Chem. Mater.* **2014**, *26*, 2829−2835.
(19) Zhang, Z. G.; Wang, J. Structures and Properties of Conjugated Donor−Acceptor Copolymers for Solar Cell Applications. *J. Mater. Chem.* **2012**, *22*, 4178−4187.
(20) Noriega, R.; Rivnay, J.; Vandewal, K.; Koch, F. P. V.; Stingelin, N.; Smith, P.; Toney, M. F.; Salleo, A. A General Relationship between Disorder, Aggregation and Charge Transport in Conjugated Polymers. *Nat. Mater.* **2013**, *12*, 1038−1044.
(21) Mei, J.; Bao, Z. Side Chain Engineering in Solution-Processable Conjugated Polymers. *Chem. Mater.* **2014**, *26*, 604−615.
(22) Coropceanu, V.; Cornil, J.; da Silva Filho, D. A.; Olivier, Y.; Silbey, R.; Brédas, J.-L. Charge Transport in Organic Semiconductors. *Chem. Rev.* **2007**, *107*, 926−952.
(23) Diao, Y.; Tee, B. C. K.; Giri, G.; Xu, J.; Kim, D. H.; Becerril, H. A.; Stoltenberg, R. M.; Lee, T. H.; Xue, G.; Mannsfeld, S. C. B.; Bao, Z. Solution Coating of Large-Area Organic Semiconductor Thin Films with Aligned Single-Crystalline Domains. *Nat. Mater.* **2013**, *12*, 665−671.
(24) Treat, N. D.; Nekuda Malik, J. A.; Reid, O.; Yu, L.; Shuttle, C. G.; Rumbles, G.; Hawker, C. J.; Chabinyc, M. L.; Smith, P.; Stingelin, N. Microstructure Formation in Molecular and Polymer Semiconductors Assisted by Nucleation Agents. *Nat. Mater.* **2013**, *12*, 628−633.
(25) Fang, L.; Zhou, Y.; Yao, Y.-X.; Diao, Y.; Lee, W.-Y.; Appleton, A. L.; Allen, R.; Reinspach, J.; Mannsfeld, S. C. B.; Bao, Z. Side-Chain Engineering of Isoindigo-Containing Conjugated Polymers Using Polystyrene for High-Performance Bulk Heterojunction Solar Cells. *Chem. Mater.* **2013**, *25*, 4874−4880.
(26) Lei, T.; Wang, J.-Y.; Pei, J. Roles of Flexible Chains in Organic Semiconducting Materials. *Chem. Mater.* **2014**, *26*, 594−603.
(27) Chen, M. S.; Niskala, J. R.; Unruh, D. A.; Chu, C. K.; Lee, O. P.; Fréchet, J. M. J. Control of Polymer-Packing Orientation in Thin Films through Synthetic Tailoring of Backbone Coplanarity. *Chem. Mater.* **2013**, *25*, 4088−4096.
(28) Wu, J.; Pisula, W.; Müllen, K. Graphenes as Potential Material for Electronics. *Chem. Rev.* **2007**, *107*, 718−747.
(29) Pisula, W.; Feng, X.; Müllen, K. Tuning the Columnar Organization of Discotic Polycyclic Aromatic Hydrocarbons. *Adv. Mater.* **2010**, *22*, 3634−3649.
(30) Xiao, J.; Duong, H. M.; Liu, Y.; Shi, W.; Ji, L.; Li, G.; Li, S.; Liu, X.-W.; Ma, J.; Wudl, F.; Zhang, Q. Synthesis and Structure Characterization of a Stable Nonatwistacene. *Angew. Chem., Int. Ed.* **2012**, *51*, 6094−6098.
(31) Schmidt-Mende, L.; Fechtenkötter, A.; Müllen, K.; Moons, E.; Friend, R. H.; MacKenzie, J. D. Self-Organized Discotic Liquid Crystals for High-Efficiency Organic Photovoltaics. *Science* **2001**, *293*, 1119−1122.
(32) Laschat, S.; Baro, A.; Steinke, N.; Giesselmann, F.; Hägele, C.; Scalia, G.; Judele, R.; Kapatsina, E.; Sauer, S.; Schreivogel, A.; Tosoni, M. Discotic Liquid Crystals: From Tailor-Made Synthesis to Plastic Electronics. *Angew. Chem., Int. Ed.* **2007**, *46*, 4832−4887.
(33) Wong, W. W. H.; Singh, T. B.; Vak, D.; Pisula, W.; Yan, C.; Feng, X.; Williams, E. L.; Chan, K. L.; Mao, Q.; Jones, D. J.; Ma, C.-Q.; Müllen, K.; Bäuerle, P.; Holmes, A. B. Solution Processable Fluorenyl Hexa-Peri-Hexabenzocoronenes in Organic Field-Effect Transistors and Solar Cells. *Adv. Funct. Mater.* **2010**, *20*, 927−938.
(34) Wu, J.-S.; Cheng, S.-W.; Cheng, Y.-J.; Hsu, C.-S. Donor-Acceptor Conjugated Polymers Based on Multifused Ladder-Type Arenes for Organic Solar Cells. *Chem. Soc. Rev.* **2015**, *44*, 1113−1154.
(35) Hoeben, F. J. M.; Jonkheijm, P.; Meijer, E. W.; Schenning, A. P. H. J. About Supramolecular Assemblies of Π-Conjugated Systems. *Chem. Rev.* **2005**, *105*, 1491−1546.
(36) Schenning, A. P. H. J.; Meijer, E. W. Supramolecular Electronics; Nanowires from Self-Assembled [Small Pi]-Conjugated Systems. *Chem. Commun.* **2005**, 3245−3258.
(37) Moulin, E.; Cid, J.-J.; Giuseppone, N. Advances in Supramolecular Electronics − from Randomly Self-Assembled Nanostructures to Addressable Self-Organized Interconnects. *Adv. Mater.* **2013**, *25*, 477−487.
(38) Xiao, S.; Zhou, H.; You, W. Conjugated Polymers of Fused Bithiophenes with Enhanced Π-Electron Delocalization for Photovoltaic Applications. *Macromolecules* **2008**, *41*, 5688−5696.
(39) Wurthner, F.; Stolte, M. Naphthalene and Perylene Diimides for Organic Transistors. *Chem. Commun.* **2011**, *47*, 5109−5115.
(40) Zhan, X. W.; Facchetti, A.; Barlow, S.; Marks, T. J.; Ratner, M. A.; Wasielewski, M. R.; Marder, S. R. Rylene and Related Diimides for Organic Electronics. *Adv. Mater.* **2011**, *23*, 268−284.
(41) Li, Y.; Xu, W.; Di Motta, S.; Negri, F.; Zhu, D.; Wang, Z. Core-Extended Rylene Dyes Via Thiophene Annulation. *Chem. Commun.* **2012**, *48*, 8204−8206.
(42) Usta, H.; Newman, C.; Chen, Z.; Facchetti, A. Dithienocoronenediimide-Based Copolymers as Novel Ambipolar Semiconductors for Organic Thin-Film Transistors. *Adv. Mater.* **2012**, *24*, 3678−3684 S3678/3671-S3678/3677..
(43) Zhou, W.; Jin, F.; Huang, X.; Duan, X.-M.; Zhan, X. A Low-Bandgap Conjugated Copolymer Based on Porphyrin and Dithienocoronene Diimide with Strong Two-Photon Absorption. *Macromolecules* **2012**, *45*, 7823−7828.
(44) Zhang, Y.; Hanifi, D.; Lim, E.; Chourou, S.; Alvarez, S.; Pun, A.; Hexemer, A.; Ma, B.; Liu, Y. Enhancing the Performance of Solution-Processed N-Type Organic Field-Effect Transistors by Blending with Molecular "Aligners. *Adv. Mater.* **2014**, *26*, 1223−1228.
(45) Zhao, J.; Wong, J. I.; Gao, J.; Li, G.; Xing, G.; Zhang, H.; Sum, T. C.; Yang, H. Y.; Zhao, Y.; Ake Kjelleberg, S. L.; Huang, W.; Joachim Loo, S. C.; Zhang, Q. Larger [Small Pi]-Extended Anti-/Syn-Aroylenediimidazole Polyaromatic Compounds: Synthesis, Physical Properties, Self-Assembly, and Quasi-Linear Conjugation Effect. *RSC Adv.* **2014**, *4*, 17822−17831.
(46) He, B.; Pun, A. B.; Klivansky, L. M.; McGough, A. M.; Ye, Y.; Zhu, J.; Guo, J.; Teat, S. J.; Liu, Y. Thiophene Fused Azacoronenes: Regioselective Synthesis, Self-Organization, Charge Transport and Its Incorporation in Conjugated Polymers. *Chem. Mater.* **2014**, *26*, 3920−3927.
(47) Dou, J.-H.; Zheng, Y.-Q.; Lei, T.; Zhang, S.-D.; Wang, Z.; Zhang, W.-B.; Wang, J.-Y.; Pei, J. Systematic Investigation of Side-Chain Branching Position Effect on Electron Carrier Mobility in Conjugated Polymers. *Adv. Funct. Mater.* **2014**, *24*, 6270−6278.
(48) Liu, Y.; Zhao, J.; Li, Z.; Mu, C.; Ma, W.; Hu, H.; Jiang, K.; Lin, H.; Ade, H.; Yan, H. Aggregation and Morphology Control Enables Multiple Cases of High-Efficiency Polymer Solar Cells. *Nat. Commun.* **2014**, *5*, 5293.
(49) Frisch, M. J.; Trucks, G. W.; Schlegel, H. B.; Scuseria, G. E.; Robb, M. A.; Cheeseman, J. R.; Scalmani, G.; Barone, V.; Mennucci, B.; Petersson, G. A.; Nakatsuji, H.; Caricato, M.; Li, X.; Hratchian, H.

DOI: 10.1021/acsami.5b04907
ACS Appl. Mater. Interfaces 2015, 7, 20034−20045

P.; Izmaylov, A. F.; Bloino, J.; Zheng, G.; Sonnenberg, J. L.; Hada, M.; Ehara, M.; Toyota, K.; Fukuda, R.; Hasegawa, J.; Ishida, M.; Nakajima, T.; Honda, Y.; Kitao, O.; Nakai, H.; Vreven, T.; Montgomery Jr., J. A.; Peralta, J. E.; Ogliaro, F.; Bearpark, M. J.; Heyd, J.; Brothers, E. N.; Kudin, K. N.; Staroverov, V. N.; Kobayashi, R.; Normand, J.; Raghavachari, K.; Rendell, A. P.; Burant, J. C.; Iyengar, S. S.; Tomasi, J.; Cossi, M.; Rega, N.; Millam, N. J.; Klene, M.; Knox, J. E.; Cross, J. B.; Bakken, V.; Adamo, C.; Jaramillo, J.; Gomperts, R.; Stratmann, R. E.; Yazyev, O.; Austin, A. J.; Cammi, R.; Pomelli, C.; Ochterski, J. W.; Martin, R. L.; Morokuma, K.; Zakrzewski, V. G.; Voth, G. A.; Salvador, P.; Dannenberg, J. J.; Dapprich, S.; Daniels, A. D.; Farkas, Ö.; Foresman, J. B.; Ortiz, J. V.; Cioslowski, J.; Fox, D. J. *Gaussian 09*, version B.01; Gaussian, Inc.: Wallingford, CT, USA, 2009.

(50) Lee, C.; Yang, W.; Parr, R. G. Development of the Colle-Salvetti Correlation-Energy Formula into a Functional of the Electron Density. *Phys. Rev. B: Condens. Matter Mater. Phys.* **1988**, *37*, 785−789.

(51) Becke, A. D. Density-Functional Thermochemistry. Iii. The Role of Exact Exchange. *J. Chem. Phys.* **1993**, *98*, 5648−5652.

(52) Miertuš, S.; Scrocco, E.; Tomasi, J. Electrostatic Interaction of a Solute with a Continuum. A Direct Utilizaion of Ab Initio Molecular Potentials for the Prevision of Solvent Effects. *Chem. Phys.* **1981**, *55*, 117−129.

(53) Tomasi, J.; Mennucci, B.; Cammi, R. Quantum Mechanical Continuum Solvation Models. *Chem. Rev.* **2005**, *105*, 2999−3094.

(54) Zhang, X.; Richter, L. J.; DeLongchamp, D. M.; Kline, R. J.; Hammond, M. R.; McCulloch, I.; Heeney, M.; Ashraf, R. S.; Smith, J. N.; Anthopoulos, T. D.; Schroeder, B.; Geerts, Y. H.; Fischer, D. A.; Toney, M. F. Molecular Packing of High-Mobility Diketo Pyrrolo-Pyrrole Polymer Semiconductors with Branched Alkyl Side Chains. *J. Am. Chem. Soc.* **2011**, *133*, 15073−15084.

(55) Gundlach, D. J.; Zhou, L.; Nichols, J. A.; Jackson, T. N.; Necliudov, P. V.; Shur, M. S. An Experimental Study of Contact Effects in Organic Thin Film Transistors. *J. Appl. Phys.* **2006**, *100*, 024509.

(56) Noda, K.; Wada, Y.; Toyabe, T. Experimental and Numerical Analysis of Channel-Length-Dependent Electrical Properties in Bottom-Gate, Bottom-Contact Organic Thin-Film Transistors with Schottky Contact. *Org. Electron.* **2014**, *15*, 3681−3687.

(57) Gundlach, D. J.; Royer, J. E.; Park, S. K.; Subramanian, S.; Jurchescu, O. D.; Hamadani, B. H.; Moad, A. J.; Kline, R. J.; Teague, L. C.; Kirillov, O.; Richter, C. A.; Kushmerick, J. G.; Richter, L. J.; Parkin, S. R.; Jackson, T. N.; Anthony, J. E. Contact-Induced Crystallinity for High-Performance Soluble Acene-Based Transistors and Circuits. *Nat. Mater.* **2008**, *7*, 216−221.

(58) Gemayel, M. E.; Treier, M.; Musumeci, C.; Li, C.; Müllen, K.; Samorì, P. Tuning the Photoresponse in Organic Field-Effect Transistors. *J. Am. Chem. Soc.* **2012**, *134*, 2429−2433.

(59) Guo, Y.; Yu, G.; Liu, Y. Functional Organic Field-Effect Transistors. *Adv. Mater.* **2010**, *22*, 4427−4447.

(60) Liu, Y.; Wang, H.; Dong, H.; Tan, J.; Hu, W.; Zhan, X. Synthesis of a Conjugated Polymer with Broad Absorption and Its Application in High-Performance Phototransistors. *Macromolecules* **2012**, *45*, 1296−1302.

(61) Liu, Y.; Shi, Q.; Ma, L.; Dong, H.; Tan, J.; Hu, W.; Zhan, X. Copolymers of Benzo[1,2-B:4,5-B′]Dithiophene and Bithiazole for High-Performance Thin Film Phototransistors. *J. Mater. Chem. C* **2014**, *2*, 9505−9511.

(62) Wang, H.; Cheng, C.; Zhang, L.; Liu, H.; Zhao, Y.; Guo, Y.; Hu, W.; Yu, G.; Liu, Y. Inkjet Printing Short-Channel Polymer Transistors with High-Performance and Ultrahigh Photoresponsivity. *Adv. Mater.* **2014**, *26*, 4683−4689.

DOI: 10.1021/acsami.5b04907
ACS Appl. Mater. Interfaces 2015, 7, 20034−20045